Progress In Electromagnetics Research C, Vol. 133, 209–218, 2023

Ground Radiation Based Triple-Band MIMO Antenna with Wideband Characteristics for Wi-Fi and Wi-Fi 6E Applications

Zeeshan Zahid[1], Ayesha Habib[1], and Longyue Qu[2, *]

Abstract—The paper presents a ground radiation antenna (GradiAnt) based triple-band MIMO antenna with wideband characteristics for Wi-Fi 6E applications. The GradiAnt is a novel antenna element with a series combination of inductor and capacitor in the feed loop, and dual-band characteristics have been achieved by controlling the impedance level of the antenna. By introducing a parasitic resonator within the feed loop of GradiAnt, triple-band characteristic is achieved, and significant bandwidth enhancement is realized, fully covering the Wi-Fi and Wi-Fi 6E operation bands. The resonator consists of a parasitic strip connected with the ground plane through an inductor. Two identical GradiAnts are symmetrically installed at the corners of the shorter edge of the $55 \times 40\,\text{mm}^2$ sized ground plane for MIMO scenarios. A loop-type isolator is installed between the antenna elements to decouple the lower Wi-Fi band where the higher bands are self-isolated. The measured bands with reference to $-6\,\text{dB}$ are 2.36–2.63 GHz and 4.76–8 GHz. The isolation in the lower and higher bands is greater than 22 dB and 17.5 dB, respectively. The ECC is less than 0.03 in the lower band and 0.16 in the higher bands.

1. INTRODUCTION

Advancing wireless terminal device applications, such as high-definition video streaming, have skyrocketed the user requirement for higher data rates [1]. Multiple-input multiple-output (MIMO) is a promising technology supporting higher channel capacity and data rate [2]. To further meet the user requirements, Wi-Fi 6E band was launched in 2021, and compatible devices are now emerging in the market [3]. The conventional antenna designs in the literature provide insufficient bandwidth for new Wi-Fi bands [4–6]. Recently, antenna researchers have proposed several novel designs for Wi-Fi 6E applications [7, 8]. In [7], a four-port square patch MIMO antenna with high port isolation was proposed for Wi-Fi 6E access points. The common-mode/differential-mode cancellation theory along with filters was utilized to design a high-isolation two-port microstrip antenna [8]. In addition, Wi-Fi 6E antennas with diverse functions were presented in [9–11]. A circularly polarized dielectric patch antenna was proposed in [9], and an omnidirectional antenna was presented in [10]. A quasi-Yagi antenna was presented in [11] for diverse radiation patterns. Although the antennas can cover Wi-Fi 6E bands, the antenna types are unsuitable for terminal devices. On the other hand, terminal antennas should be designed by addressing compactness and high radiation performance simultaneously. Electrically small antennas embedded in the ground plane of a terminal device usually suffer from narrow impedance bandwidth and low radiation efficiency [12]. Therefore, ground radiation antennas (GradiAnts) have been proposed as electrically small antennas embedded in an electrically larger ground plane. The GradiAnts excite the ground plane as a real radiator [13–15]. Moreover, various bandwidth enhancement techniques of mobile device antennas have been proposed in the literature [10, 16–18]. For instance, a

Received 17 April 2023, Accepted 30 May 2023, Scheduled 7 June 2023

* Corresponding author: Longyue Qu (qulongyue@hit.edu.cn).

[1] Department of Electrical Engineering, College of Signals, National University of Sciences and Technology, Rawalpindi, Pakistan.

[2] Department of Electronics and Information Engineering, Harbin Institute of Technology (Shenzhen), Shenzhen, China.

parallel resonant feed structure can be used to produce additional resonance into the antenna so that wideband characteristics were obtained in either single-band or dual-band applications [16–18]. However, the main disadvantage lies in their complex tuning process. In the case of MIMO antennas, the isolator design plays a critical role in the MIMO antenna performance [19, 20], and a loop-type isolator has been employed in various studies [21, 22]. Accordingly, MIMO antennas with wideband characteristics, high isolation, and high radiation performance are in desperate need of modern Wi-Fi 6E applications. Nevertheless, terminal antennas intended for Wi-Fi 6E applications have been reported in [23–27]. To the best of our knowledge, an embedded dual-band antenna achieving more than 3 GHz bandwidth has not been reported in the literature yet. The comparison with the state-of-the-art antennas of wireless terminal devices proposed in the literature is given in Table 1 to address the novelty and advancement of this study.

Table 1. Comparison with the state-of-the-art literature.

Refs.	Element size (mm^2)	Antenna type	Bandwidth (GHz)	Max. Isolation (dB)	Efficiencies (%)	ECC	DG
[23]	18×6	MIMO	2.4–2.484 and 5.15–7.125	12.5 and 16	71 and 82	< 0.5	Not given
[24]	43×3	Single	2.4–2.484 and 5.15–7.125	N.A	68 and 63	Invalid	Invalid
[25]	17.8×3	Single	2.4–2.49 and 4.35–7.61	N.A	> 40 and > 61	Invalid	invalid
[26]	14.5×5	MIMO	2.4–2.49 and 5.925–7.125	20 and 16	60 and > 80	< 0.02 and < 0.04	Not given
[27]	30×6	MIMO	2.4–2.49 and 4.8–7.4	13 and 14	70 and 86	< 0.22 and < 0.04	Not given
Prop.	10.5×4	MIMO	2.36–263 and 4.76–8	22 and 17	64 and 84	< 0.03 and < 0.2	> 9.85

The design given in [23] is for smartphone applications whereas the studies of [24–27] are for laptop applications. It is evident from the table that the size of the proposed antenna element is smaller than the other designs, and the achieved bandwidth and isolation performance of the proposed design is better than the other antennas. Moreover, the efficiency performance in the lower band is better than [24, 25] whereas in the higher band the efficiency is better than [23–26]. Therefore, the main contribution of this study is to propose a simple and novel bandwidth enhancement technique and a high-performance isolator for wideband Wi-Fi 6E MIMO antennas, having the advantages of compactness and tunability. In this paper, we propose a triple-band GradiAnt with wideband characteristics for modern Wi-Fi and Wi-Fi 6E applications. Dual-band characteristics have been achieved by a series combination of inductor and capacitor in the feed loop that controls the impedance level of the antenna. An additional operation band was obtained by using a parasitic resonator in the feed loop so that the bandwidth of the higher Wi-Fi band is significantly enhanced. The design is extended to a 2×2 MIMO antenna system where a loop-type resonator is employed to isolate the lower band for high isolation property. Both simulation and measurement were conducted to validate the proposed technique.

2. ANTENNA CONFIGURATION AND OPERATION MECHANISM

The geometry of the proposed antenna is displayed in Figure 1. The size of the ground plane is $55 \times 40\,mm^2$ where FR4 ($\epsilon_r = 4.4$, $\tan(\delta) = 0.02$, thickness = 1 mm) is used as a substrate material. The size of the ground plane is selected for Modern TV remotes supporting Wi-Fi 6e bands. The

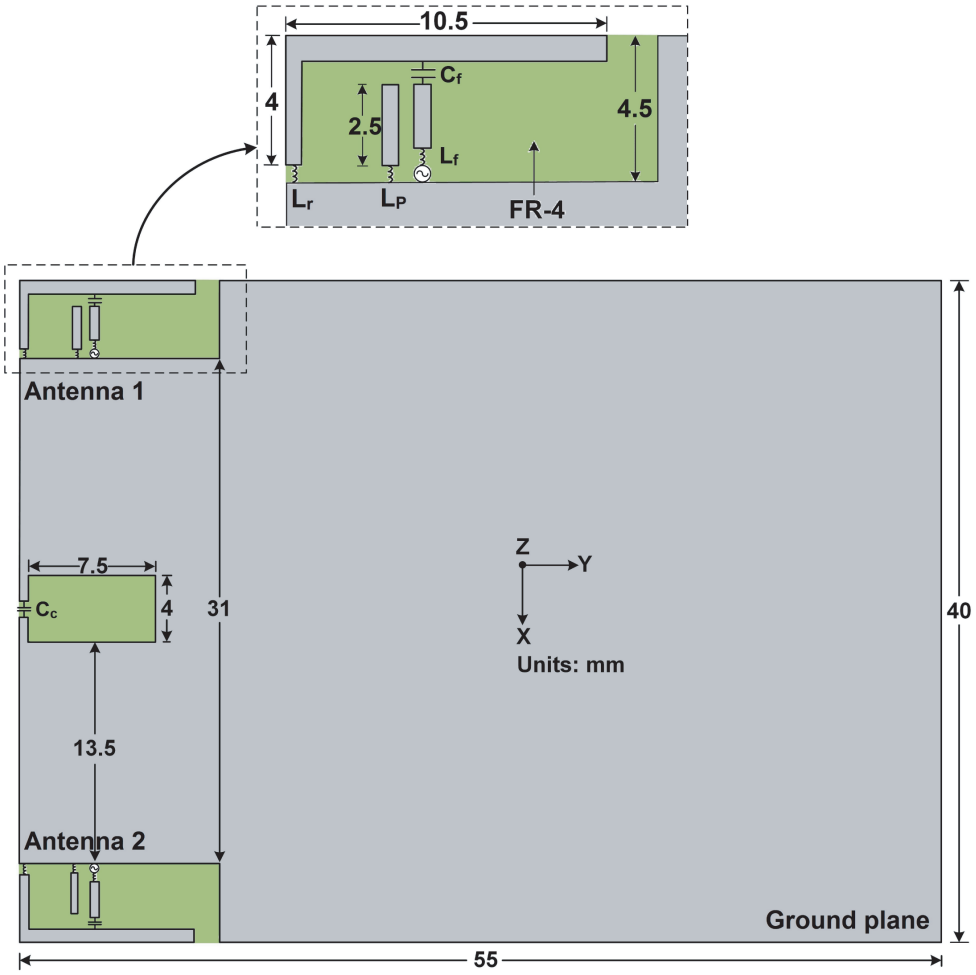

Figure 1. Geometry of the proposed MIMO antenna.

antenna elements have been designed within $12 \times 4.5\,\text{mm}^2$ sized clearances etched at the left corner of the ground plane. Each antenna element consists of a GradiAnt where the length of the radiation strip is 12 mm. The radiation strip is connected with the ground plane through an inductor (L_r). The resonance frequencies of the antenna are tuned by the length of the radiation strip and L_r. Increasing the value of L_r reduces the first resonance frequency and vice versa. The GradiAnt is fed by a feed strip that contains a feed capacitor (C_f) and a feed inductor (L_f). Dual-band performance is achieved using a series configuration of L_f and C_f in the feed loop that controls the impedance level of the antenna. The effect of changing the values of the lumped elements of the PIFA antenna has been discussed in various studies such as [17–19]. In order to increase the bandwidth of the higher band, a parasitic resonator is introduced within the feed loop. The resonator consists of a strip of length 2.5 mm, connected with the ground plane through an inductor (L_p). Both antenna elements have been installed at the left corners of the ground plane. The design without the isolator is designated as the reference antenna. A capacitively coupled loop-type isolator is installed between the antenna elements to reduce the coupling in the lower band. The isolation frequency can be tuned by adjusting the decoupling capacitor C_c. Increasing the value of C_c decreases the isolation frequency and vice versa. A loop-type structure acts as a magnetic coupler that shows maximum coupling where the current density of the dominant ground mode is maximum. The coupling can be expressed as [28],

$$\alpha_m = \frac{-1}{1 + j\lambda} \iiint H^g \cdot M^i d\tau \tag{1}$$

where M_i is the impressed magnetic current density, and H^g is the magnetic field produced by the characteristic mode of the nth ground mode. The eigenvalue of the nth ground mode is represented by λ_n. In the ground radiation antennas, the antenna element acts as the excitation whereas the ground plane acts as the main radiator. The size of the ground plane determines the resonance frequency of the ground mode. Therefore, the size of the ground plane definitely affects the radiation performance. Characteristic mode analysis of the ground plane reveals that the dominant ground mode is resonant close to the lower Wi-Fi band and shows minimum current at the side edges of the ground plane. To achieve higher radiation efficiency, the isolator is placed at the proposed location where it exhibits minimal coupling with the dominant ground mode [19].

3. SIMULATION RESULTS

Firstly, full-wave simulations were conducted to optimize the GradiAnt design for the desired bandwidth. The optimized values of C_f, L_f, L_r, and L_P are 0.17 pF, 1.6 nH, 1.7 nH, and 1 nH, respectively. The impact of the parasitic resonator on the return loss is presented in Figure 2 where shaded areas represent the Wi-Fi and Wi-Fi 6E bands. The figure reveals that without the parasitic resonator, the GradiAnt exhibits dual-band characteristics where the 2.45 GHz band is fully covered. However, the higher band does not cover the Wi-Fi 6E band, as expected. The introduction of the parasitic strip produces additional resonance in the higher band that can be tuned using L_p. As demonstrated in Figure 2, increasing the value of L_p lowers the parasitic resonance frequency without affecting the lower two resonances. Therefore, L_p can be optimized to achieve triple band characteristics having more than 3 GHz bandwidth at the higher Wi-Fi band. It is evident that the advantage of the proposed technique lies in the huge bandwidth enhancement without increasing the size of the antenna and without affecting the original resonances of the ground mode. Furthermore, the simulated S-parameters of the reference and proposed antennas are compared in Figure 3. The graph shows that the lower band exhibits higher coupling (-10 dB approx.) between the GradiAnts whereas the coupling in the higher bands is lower than -15 dB. Therefore, the loop-type isolator is employed to increase the isolation in the lower band. The effect of the isolator can be observed by analyzing the current distribution. Figure 4 presents the simulated current distribution on the ground plane at 2.45 GHz when Antenna 1 was excited, and Antenna 2 was terminated at the matched load. Figure 4 shows that the current is strongly coupled with the loop-type isolator, resulting in a lower current density at Antenna 2. The length of the ground plane is approximately half of the wavelength at 2.45 GHz. Therefore, the halfwave mode is excited along the y-axis. Figure 5 shows the current distribution at 6 GHz. Even though the isolator is uncoupled, the current coupled with Antenna 2 is weaker due to the larger electrical distance between the antennas. The length of the ground plane is approximately one wavelength at 6 GHz. Therefore, the full-wave mode is excited along the y-axis as shown in Figure 5.

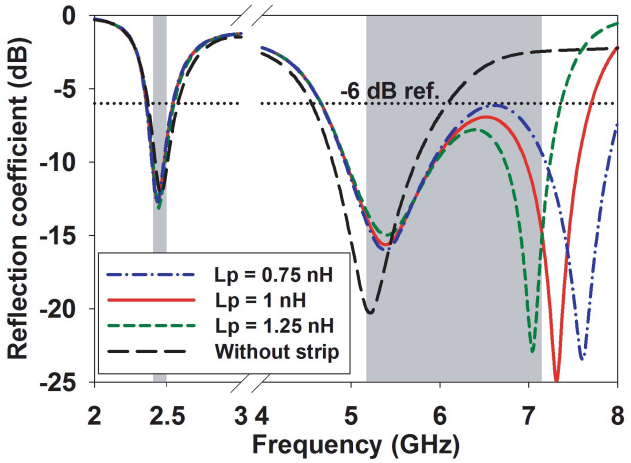

Figure 2. The impact of the parasitic strip and the value of L_p on reflection coefficient.

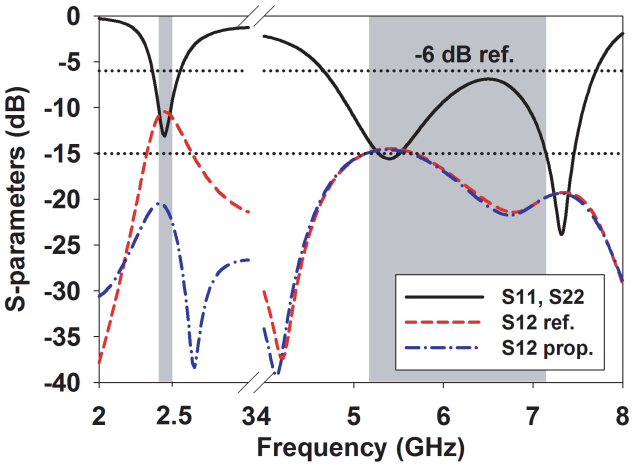

Figure 3. The effect of loop-type isolator on S-parameters.

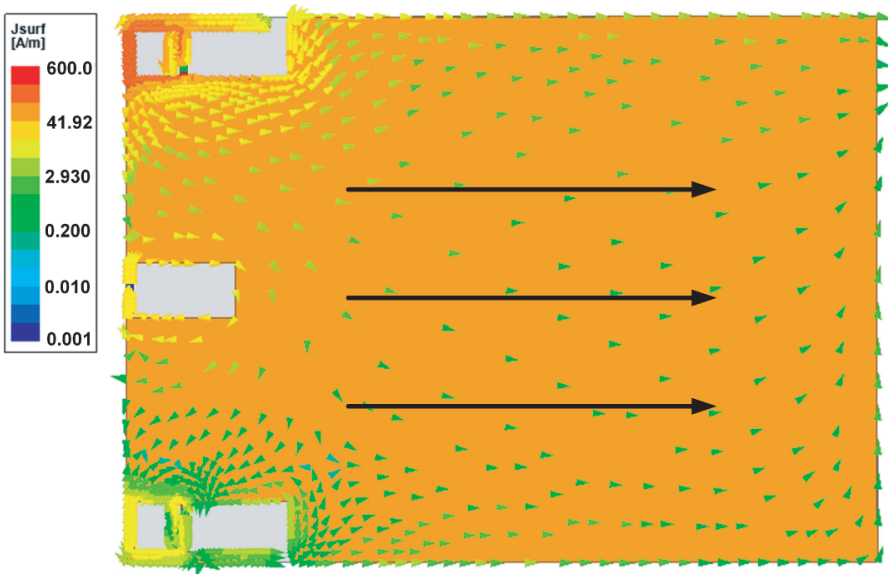

Figure 4. The simulated current density at 2.45 GHz.

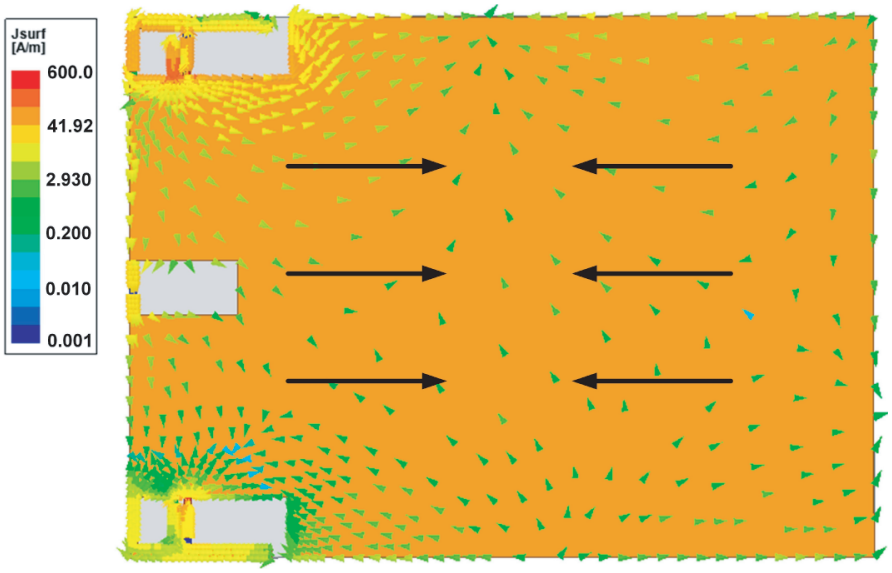

Figure 5. The simulated current density at 5.5 GHz.

4. MEASURED RESULTS

The proposed antenna was fabricated, as pictured in Figure 6, to validate the simulation results. Figure 7 shows the comparison of measured and simulated S-parameters. The measured impedance bandwidths of both antennas are 270 MHz (2.36–2.63 GHz) and 3.24 GHz (4.76–8 GHz). The parasitic resonator is tuned at 7.5 GHz to achieve wider matching bandwidth. The isolation in the lower band is greater than 22 dB indicating the effective operation of the loop-type isolator. The higher band exhibits more than 17 dB isolation.

The radiation patterns of the MIMO antennas were measured in a 3D CTIA-OTA chamber at 2.45 GHz, 5.5 GHz, and 6.5 GHz frequencies. The measured and simulated radiation patterns of the

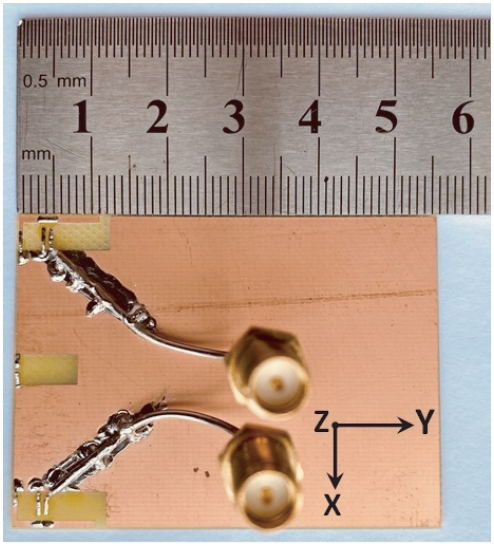

Figure 6. The fabricated antenna.

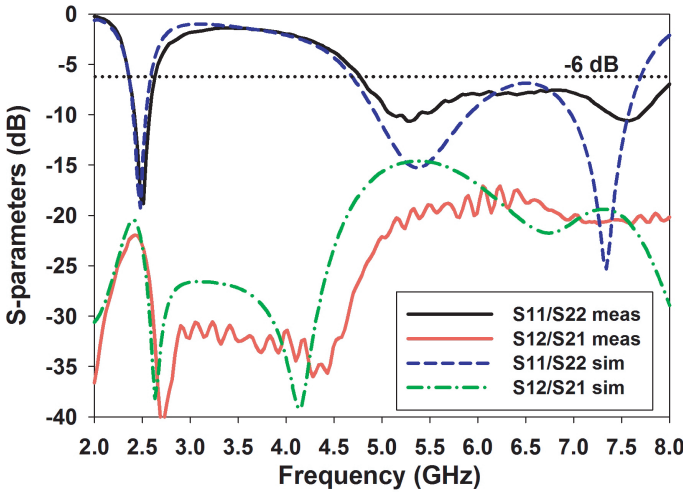

Figure 7. The measured and simulated S-parameters.

Table 2. Measured peak gains at different frequencies.

Freqs.	Antenna 1 (dB)	Antenna 2 (dB)
2.45 GHz	1.27	1.46
5.5 GHz	1.42	1.6
6.5 GHz	1.43	1.92

antennas are presented in Figure 8. The peak values of the measured gain at the frequencies are tabulated in Table 2. The data indicates that the gain increases slightly with frequency. The peak values of total radiation efficiencies in the lower and higher bands are 64% and 84%, respectively. To further validate the diversity performance of the proposed antennas, the envelope correlation coefficient (ECC) and diversity gain (DG) are discussed here. ECC is a critical parameter that indicates the diversity performance of the MIMO antenna. ECC was calculated using the measured pattern data by the following expression [29],

$$ECC = \frac{|\iint_{4\pi} F_1(\theta,\phi)F_2(\theta,\phi)d\Omega|^2}{\iint_{4\pi}|F_1(\theta,\phi)|^2 d\Omega \iint_{4\pi}|F_2(\theta,\phi)|^2 d\Omega} \tag{2}$$

where $F_i(\theta,\phi)$ represents the radiation pattern of the MIMO antenna when the ith port is excited. The measured total efficiencies and ECC are shown in Figure 9 where it can be observed that the ECC values are well below 0.2 in the operating bands. The DG can be calculated using the following equation [30],

$$DG = 10\sqrt{1 - ECC^2} \tag{3}$$

The measured DG values are presented in Figure 10. The data depict that the DG is approximately 10 in the lower band and greater than 9.85 in the higher band, indicating good MIMO performance. The antenna mainly possesses triple-band characteristics, evident from Figures 2 and 3. However, the 2nd and 3rd resonances have been adjusted to achieve wideband characteristics so that the Wi-Fi 6e band is covered. Therefore, the combined effect appears as dual-band characteristics in Figures 7, 9, and 10.

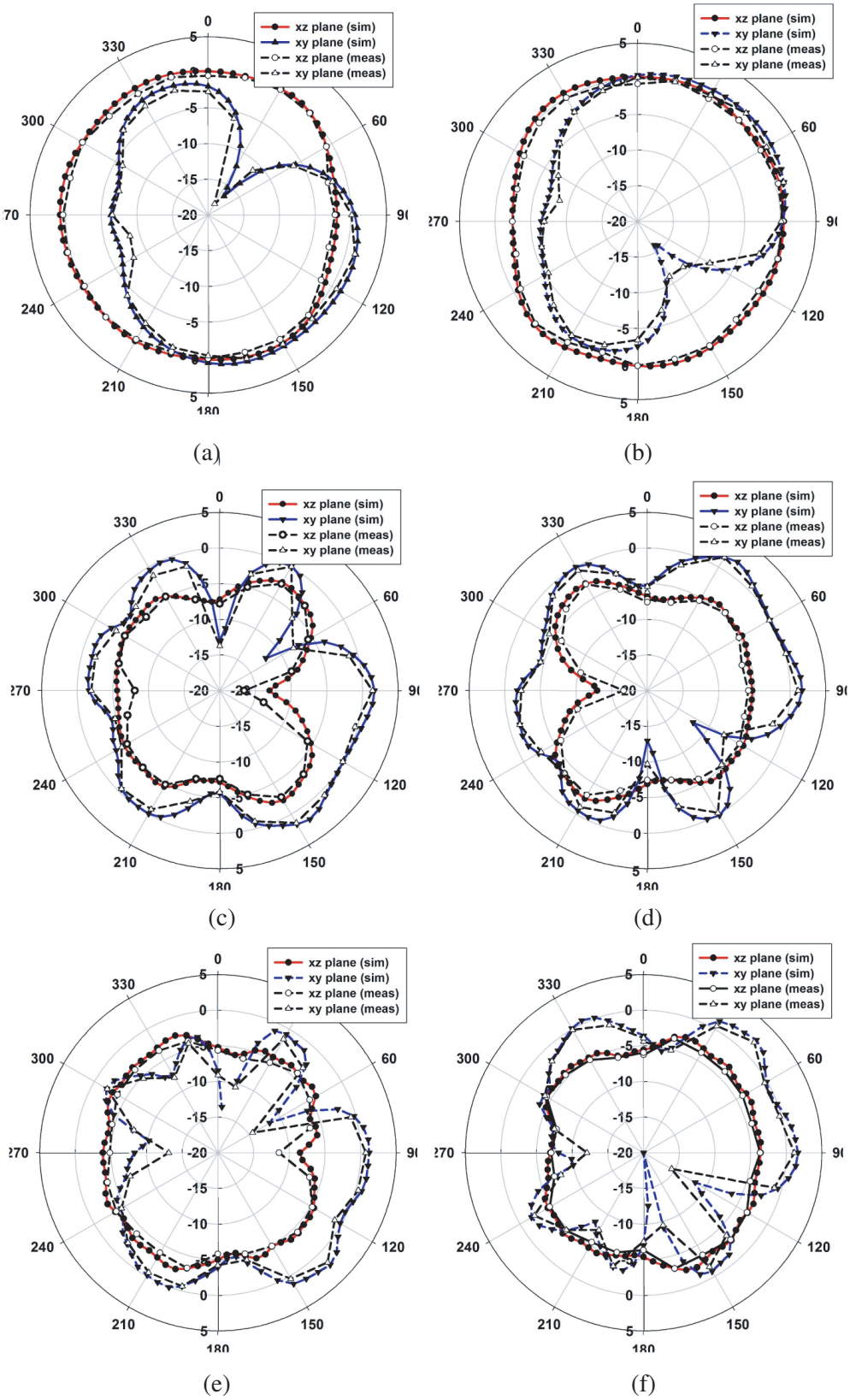

Figure 8. Simulated and measured radiation patterns of Antenna 1 at (a) 2.45 GHz, (c) 5.5 GHz, (e) 6.5 GHz, Antenna 2 at (b) 2.45 GHz, (d) 5.5 GHz and (f) 6.5 GHz.

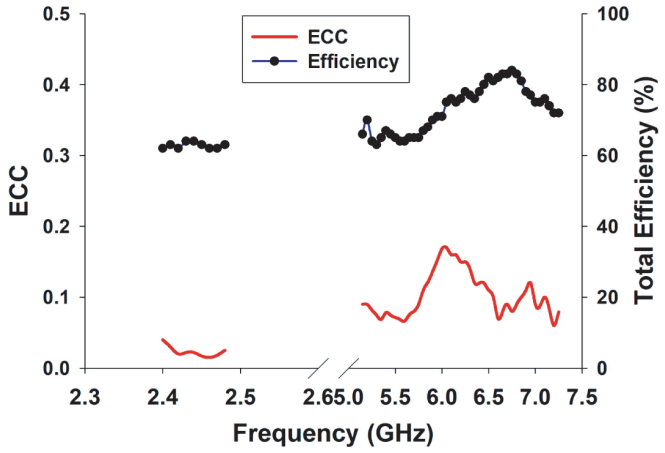

Figure 9. Measured total efficiencies and ECC of the MIMO antenna.

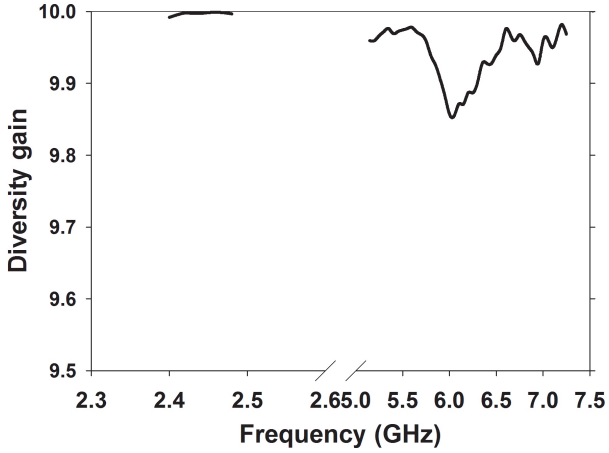

Figure 10. The measured diversity gain of the MIMO antenna.

5. CONCLUSION

In this work a triple-band GradiAnt MIMO antenna has been proposed with wideband characteristics for Wi-Fi 6E applications. A novel GradiAnt element with a parasitic resonator in the feed loop was proposed, achieving 270 MHz and 3.24 GHz bandwidths in the lower and higher bands, respectively. The noteworthy aspect of the proposed design is that triple-band and wideband performance is realized without increasing the antenna size and without sacrificing the original dual-resonances. The MIMO antennas were constructed where a loop-type isolator was employed so that the isolation is higher than 21 dB and 17 dB in the lower and higher bands, respectively. The measured peak efficiencies in the lower and higher bands were 64% and 84%, respectively. The ECC in both bands was less than 0.2, and the diversity gain was higher than 9.85. The compactness, wide bandwidth, and good MIMO performance are the key features making the proposed design a good candidate for future Wi-Fi 6E devices.

REFERENCES

1. Sim, C., H. Liu, and C. Huang, "Wideband MIMO antenna array design for future mobile devices operating in the 5G NR frequency bands n77/n78/n79 and LTE band 46," *IEEE Antennas and Wireless Propagation Letters*, Vol. 19, No. 1, 74–78, 2020.
2. Foschini, G. J. and M. J. Gans, "On limits of wireless communication in a fading environment when using multiple antennas," *Wireless Personal Commun.*, Vol. 6, 311–335, 1998.
3. https://www.lairdconnect.com/rf-antennas/wifi-antennas/internal-ntennas/flexpifa-flexpifa-6e-flexible-adhesive-backed-pifa-internal-antennas.
4. Guo, J., H. Bai, A. Feng, Y. Liu, Y. Huang, and X. Zhang, "A compact dual-band slot antenna with horizontally polarized omnidirectional radiation," *IEEE Trans on Antennas and Propag.*, Vol. 20, No. 7, 1234–1238, 2021.
5. Brocker, D. E., Z. H. Jiang, M. D. Gregory, and D. H. Werner, "Miniaturized dual-band folded patch antenna with independent band control utilizing an interdigitated slot loading," *IEEE Trans on Antennas and Propag.*, Vol. 65, No. 1, 380–384, 2017.
6. Cui, Y., X. Wang, G. Shen, and R. Li, "A triband SIW cavity-backed differentially fed dual-polarized slot antenna for WiFi/5G applications," *IEEE Trans. on Antennas and Propag.*, Vol. 68, No. 12, 8209–8214, 2020.

7. Wong, K.-L., H.-Y. Jiang, and W.-Y. Li, "Decoupling hybrid metal walls and half-wavelength diagonal open-slots based four-port square patch antenna with high port isolation and low radiation correlation for 2.4/5/6 GHz WiFi-6E 4×4 MIMO Access Points," *IEEE Access*, Vol. 10: 81296–81308, 2022.
8. Zhang, W., Y. Li, K. Wei, and Z. Zhan, "A two-port microstrip antenna with high isolation for Wi-Fi 6 and Wi-Fi 6E applications," *IEEE Transactions on Antennas and Propag.*, Vol. 70, No. 7, 5227–5234, 2022.
9. Jiang, H., N. Yan, K. Ma, and Y. Wang, "A wideband circularly polarized dielectric patch antenna with a modified air cavity for Wi-Fi 6 and Wi-Fi 6E applications," *IEEE Antennas and Wireless Propagation Letters*, Vol. 22, No. 1, 213–217, 2023.
10. Cao, Z., K. Wei, and Z. Zhang, "Low-cost compact omnidirectional antenna for tri-band Wi-Fi 6E applications," *Microwave and Optical Technology Letters*, Vol. 64, No. 11, 2052–2058, 2022.
11. Cao, Z., K. Wei, and Z. Zhang, "Low-cost compact omnidirectional antenna for tri-band Wi-Fi 6E applications," *Microwave and Optical Technology Letters*, Vol. 64, No. 11, 2052–2058, 2022.
12. Wheeler, A. H., "Small antennas," *IEEE Trans on Antenna Propag.*, Vol. 23, 462–469, 1975.
13. Liu, Y., H.-H. Kim, and H. Kim, " Loop-type ground radiation antenna for dual-band WLAN applications," *IEEE Trans. Antennas Propag.*, Vol. 61, No. 9, 4819–4823, 2013.
14. Zahid, Z. and H. Kim, "Analysis of a loop type ground radiation antenna based on equivalent circuit model," *IET Microw. Antennas Propag.*, Vol. 11, No. 1, 23–28, 2016.
15. Qu, L., Z. Zahid, H.-H. Kim, and H. Kim, "Circular polarized ground radiation antenna for mobile applications," *IEEE Trans. Antennas Propag.*, Vol. 66, No. 5, 2655–2660, 2018.
16. Jeon, S., Y. Liu, S. Ju, and H. Kim, "PIFA with parallel resonance feed structure for wideband operation," *Electronics Letters*, Vol. 47, No. 23, 1263–1265, 2011.
17. Lee, J., Y. Liu, and H. Kim, "Mobile antenna using multi-resonance feed structure for wideband operation," *IEEE Trans. Antennas Propag.*, Vol. 62, No. 11, 5851–5855, 2014.
18. Lee, J. and H. Kim, "Miniaturized WLAN antenna in mobile handset with wide impedance bandwidth characteristic," *Microwave and Optical Technology Letters*, Vol. 55, No. 12, 2841–2844, 2013.
19. Lee, H., J. Jihwan, D. Park, H. Shin, and H. Kim, "MIMO antenna performance with isolator," *Microwave and Optical Technology Letters*, Vol. 55, No. 5, 946–952, 2022.
20. Zahid, Z., L. Qu, H. H. Kim, and H. Kim, "Decoupler design for MIMO antennas of USB dongle applications using ground mode coupling analysis," *Progress In Electromagnetics Research M*, Vol. 76, 113–22, 2018.
21. Qu, L., R. Zhang, and H. Kim, "Decoupling between ground radiation antennas with ground-coupled loop-type isolator for WLAN applications," *IET Microw. Antennas Propag.*, Vol. 10, 546–552, 2016.
22. Baloch, B. A., L. Qu, Z. Zahid, and A. A. Khan, "A wideband decoupling method using bezel-coupled loop-type isolator for smartwatch MIMO applications," *International Journal of Microwave and Wireless Technologies*, 1–11, 2022.
23. Cai, A., K.-Y. Kai, and W.-J. Liao, "A WLAN/WiFi-6E MIMO antenna design for handset devices," *2021 International Symposium on Antennas and Propagation (ISAP)*, 2021.
24. Jhang, W.-C. and J.-S. Sun, "Small antenna design of triple band for WIFI 6E and WLAN applications in the narrow border laptop computer," *International Journal of Antennas and Propagation*, 2021.
25. Sim, C.-Y.-D., J. Kulkarni, S.-H. Wang, S.-Y. Zheng, Z.-H. Lin, and S.-C. Chen, "Low profile laptop antenna design for Wi-Fi 6E band," *IEEE Antennas and Wireless Propagation Letters*, Vol. 22, No. 1, 79–83, 2023.
26. Su, S.-W., D. P. Yusuf, and F.-H. Chu, "Conjoined, Wi-Fi 6E MIMO antennas for laptops," *2021 International Symposium on Antennas and Propagation (ISAP)*, 2021.
27. Su, S.-W. and C.-C. Wan, "Asymmetrical, self-isolated laptop antenna in the 2.4/5/6 GHz Wi-Fi 6E bands," *International Symposium on Antennas and Propagation (ISAP)*, 2021.

28. Harrington, R. F., *Time Harmonic Electromagnetics*, 2nd Edition, Wiley IEEE Press, 2001.
29. Vaughan, R. G. and J. B. Andersen, "Antenna diversity in mobile communications," *IEEE Trans. Veh. Technol.*, Vol. 36, 149–172, 1987.
30. Zahra, H., W. A. Awan, A. W. Hussain, S. M. Abbas, and A. A. Mukhopadhyay, "28 GHz broadband helical inspired end-fire antenna and its MIMO configuration for 5G pattern diversity applications," *Electronics*, Vol. 10, 405, 2021.